NRC Research Press

ARTICLE

Vibrational signatures of chemical- and density-induced structural changes in simulated amorphous silica[1]

Victoria R. Grandy, Kristin M. Poduska, and Ivan Saika-Voivod

Abstract: Molecular dynamics simulations show that vibrational modes in glassy SiO_2 are affected differently by density-induced changes to the structural order compared with those induced by specific cationic substitutions (Al, P, Na). Using standard measures of local and midrange positional order, we find that P disrupts network order in terms of second nearest neighbours, but preserves local order. In contrast, Al decreases local order while maintaining network order. Increased density preserves structural correlations in the network although the length scale shrinks. The complex short-range and long-range structural trends in these modified glasses coincide with changes in distinct regions in the vibrational density of states (VDOS). This suggests that a greater role for VDOS as a tool to link simulation and experiment in amorphous materials.

PACS Nos.: 61.43.Bn, 61.43.Fs, 63.50.Lm.

Résumé : Des simulations de dynamique moléculaire montrent que les modes de vibration dans le SiO_2 vitreux sont affectés différemment par les changements induits par la densité à l'ordre structural comparés à ceux induits par des substitutions cationiques spécifiques (Al, P, Na). Utilisant des mesures standard d'ordre de positionnement à courte et moyenne portée, nous trouvons que P perturbe le réseau (de verre) au niveau des deuxièmes voisins, mais laisse intact l'ordre local, alors que Al perturbe l'ordre local et laisse l'ordre du réseau intact. Une augmentation de la densité préserve les corrélations structurelles du réseau, même si l'échelle de longueur diminue. Les tendances structurelles complexes à courte et à longue portée dans ces verres modifiés coïncident avec des changements dans des régions distinctes dans les densités d'états de vibration (VDOS). Ceci suggère que VDOS peut jouer un plus grand rôle pour lier simulations et expérimentation dans les matériaux amorphes. [Traduit par la Rédaction]

1. Introduction

Glasses are inherently aperiodic materials, yet this lack of three-dimensional periodicity does not mean that they lack order. For example, there can be very good local order in a well-formed glass. While there are well-established experimental tools that can probe the two extremes of local order (e.g., X-ray absorption fine structure) and long-rage periodicity (e.g., diffraction), it is an ongoing challenge to quantify changes to the midrange order in materials, regardless of whether they are glassy or crystalline [1, 2]. Vibrational properties are one assessment method that can span from local to long-range effects, yet vibrational density of states (VDOS) is not the primary tool in theoretical studies of glasses. Midrange order differences are important because they have been implicated in many important material behaviours including crystallization–devitrification products [3, 4], links between polymorphism and polyamorphism [5, 6], dissolution trends [7], and as signatures of material formation processes [8].

In this work, we look to the vibrational properties of simulated glassy liquids as a first step toward identifying structural features in amorphous materials that are indicative of changes in midrange order. To do this, we present molecular dynamics simulations of chemically simple (silicate) liquids and compare differences that appear in their VDOS. We make a general distinction between local modes (higher wavenumbers) and extended or lattice modes (lower wavenumber) regions, and how each range is affected by either mechanically induced (density related) structural changes or by the addition of either network-forming or network-disrupting chemical defects. Our results demonstrate that chemical substitutions have complex structural affects that can affect long-range and short-range order differently, even in very simple cases.

2. Context

Defects in glasses can have several different origins. Chemical additives, impurities, or dopants are typically classified as either network forming (such as B, Ge) or network disrupting (such as Na or other alkali metals or alkaline earth metals).

Tracking defects in solids is typically an easier task in simulated systems [9], wherein ring analyses can be used to track connectivity differences. Measures of positional order, such as the structure factor, $S(q)$, for long-range effects and the radial distribution function, $g(r)$, for local order, can be measured by scattering and nuclear magnetic resonance spectroscopy [3], and they can also be obtained from simulation [10].

VDOS is an underused quantity in computational studies, and yet it offers interesting opportunities to match with experiment. Density-related and impurity-related defects have been widely studied in the context of ion diffusion, but there has been substantially less work related to their effect on vibrational properties. The VDOS cannot be assessed with a single experimental measurement; infrared spectroscopy will detect only modes that have a change in dipole moment, and Raman scattering spectroscopy will detect only modes with polarizability changes. There have been a few experimental studies that have combined Raman and infrared data to produce an effective VDOS [11]. Other experimental studies have focused on spectroscopic measures of vibrational properties as a function of temperature [12, 13].

Received 25 October 2013. Accepted 6 January 2014.

V.R. Grandy, K.M. Poduska, and I. Saika-Voivod. Department of Physics and Physical Oceanography, Memorial University of Newfoundland, St. John's, NL A1B 3X7, Canada.

Corresponding author: K.M. Poduska and I. Saika-Voivod (e-mails: kris@mun.ca, saika@mun.ca).

[1]This paper was presented at the 25th International Conference on Amorphous and Nanocrystalline Semiconductors (ICANS25).

Fig. 1. A schematic representation of (*a*–*d*) the contributions of four selected Si–O vibrational modes within a single SiO_4 tetrahedron to (*e*) specific VDOS features. Modes (*a*) and (*b*) are directed along the Si–O bond axes, while (*c*) and (*d*) are lower-energy twisting modes.

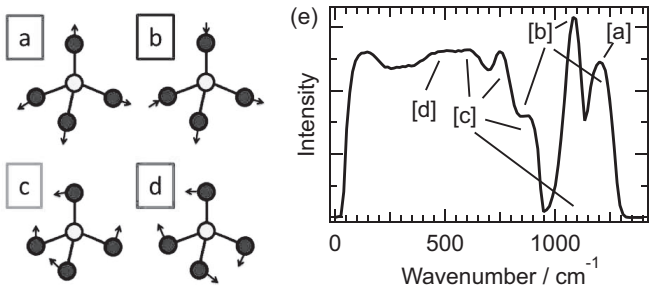

Work by others [14, 15] has shown that the VDOS for silica can be partitioned among different vibrational modes, as illustrated in Fig. 1. In this work, we focus on two specific regions of interest. The first is 1000–1200 cm^{-1}, which includes the two highest energy peaks that are derived primarily from modes that are along-axis Si–O bond vibrations with a distinct local character (Figs. 1*a* and 1*b*). This region is the only one that is dominated by local modes that affect the dilation of individual tetrahedra. The second region is 800–950 cm^{-1}, which contains a shoulder that is almost exclusively related to twisting modes (Fig. 1*c*) that affect the relative orientation of the tetrahedra, rather than their volume, and are thus more strongly affected by the connectivity of the SiO_4 tetrahedra. While there are other VDOS peaks at lower energy that are also related to network connectivity and lattice modes, this shoulder is the only region that has a dominant contribution from a single twisting mode. To summarize, we associate disruptions in local order with changes between 1000–1200 cm^{-1}, and we attribute differences in network connectivity to changes in the shoulder near 850 cm^{-1}. Our work will show that simple distinctions in the VDOS data show qualitative trends that correlate well with the more standard quantitative measures of local positional order $g(r)$ and its integral $n(r)$, and long-range positional order $S(q)$.

3. Computational details

We carry out molecular dynamics simulations using GROMACS v4.5.5 [16–19]. Pure liquid silica (SiO_2) simulations employ the van Beest – Kramers – van Santen potential [20] for a system of 444 SiO_2 units in a cubic simulation cell with periodic boundary conditions at eight densities: 2.31, 2.45, 2.61, 2.80, 3.01, 3.26, 3.55, and 3.90 g/cm^3. All simulations are carried out at T = 3000 K using the Nosé–Hoover thermostat with a time constant of 1 ps. The radial cutoff is 1 nm for all real space pair interactions. Coulomb interactions are handled with the particle mesh Ewald algorithm with a Fourier spacing of 0.1 nm and interpolation of order four (cubic). We add to the van Beest – Kramers – van Santen potential a short range interaction, described in ref. 21, to prevent the system from exploring the unphysical attraction occurring at small distances. At this T, the model exhibits glassy dynamics and at the lowest densities, the tetrahedral network is well formed, resulting in an approach to Arrhenius dynamics [21-23]. The simulations are carried out for 6 ns, sufficient to equilibrate the least diffusive state point (2.31 g/cm^3), for which Si ions diffuse an average distance of 0.31 nm (one Si–Si distance) in roughly 2.5 ns.

Substitutional impurities are gradually added to the 2.31 g/cm^3 system by replacing Si ions in such number ratios as to preserve charge balance. For example, five Si ions are replaced by 12 Na ions before simulating for another 6 ns. The simulations with impurities are carried out at a constant pressure of –1.6 GPa to match the conditions at 2.31 g/cm^3 for this silica model. The constants used for the pair potentials for the impurity ions are taken from ref. 24. We note the partial charges for the cations: 2.40 for Si, 1.40 for Al, 3.40 for P, and 1.00 for Na. We report results for which there are 60 impurity ions.

Fig. 2. VDOS changes as a function of (*a*) different substitutional impurities or (*b*) increasing density. Arrows indicate the general trends as a function of increasing density.

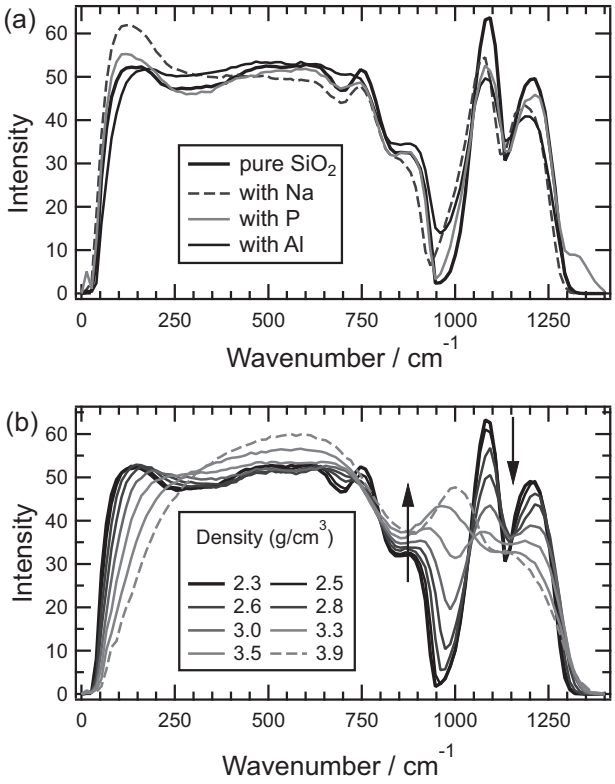

To obtain VDOS, configurations drawn from the liquid are each quenched, using the conjugate gradient algorithm, to a local potential energy minimum. At this minimum, the mass-weighted Hessian is evaluated and diagonalized, with the spectrum of eigenfrequencies yielding the VDOS. GROMACS conveniently provides utilities to carry out these calculations. To characterize the structure of the liquids, we calculate the partial Si–Si structure factor, $S(q)$, the radial distributions function, $g(r)$, and its integral, $n(r)$, to get the number of atoms in the coordination sphere of radius r. The radial distribution function, $g(r)$, gives the dimensionless orientational average of local positional order, while $S(q)$, related to the Fourier transform of $g(r)$, indicates periodicities in density fluctuations [25].

4. Results and discussion

Figure 2 shows noticeable changes in the VDOS when we either increase the density (in compositionally pure silica) or change the type of substitutional impurity (in silica equilibrated at a constant pressure). In all cases, the peaks between 1000 and 1200 cm^{-1} show slight energy shifts and decreases in intensity. These peaks show a more considerable change in intensity as density increases, but with no significant change in position until the highest densities. We note that this is a very large range of densities. For the shoulder near 850 cm^{-1}, P preserves the intensity, Na attenuates it, while Al impurities cause it to increase in a way that is similar to the effect of increasing density.

We note that the peak near 100 cm^{-1} is consistent with a Boson peak that is typically observed in silica and other glass forming

Fig. 3. $n(r)$ and $g(r)$ for different impurities for (*a*) Si–O, (*b*) impurity–O, (*c*) $g(r)$ for in Si–impurity pairs, and (*d*) Si–O as a function of density. In (*d*), arrows track the increase in density.

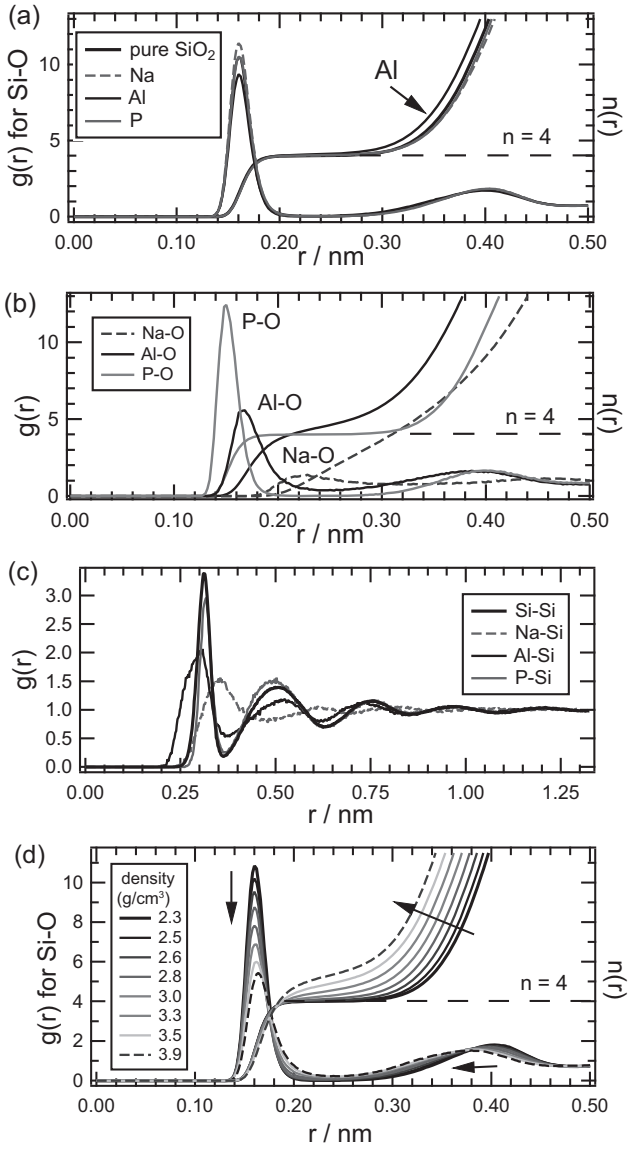

materials. Its origins are still debated, but it is generally attributed to modes associated with the SiO_4 tetrahedral units [26, 27]. Recent work by others has shown that Na contributes greatly to this low-energy peak in MD simulations of Na-containing silica glasses [28]. However, we will not discuss the changes in this particular region of the VDOS spectra in detail here.

Based on these comparisons, it appears that the VDOS can tell us very quickly about some important effects induced by different perturbations to the pure SiO_2 glass. First, all perturbations decrease the short-range order in the system, which we infer from the decreased peak intensities at 1200 and 1100 cm^{-1}. Second, and perhaps more interestingly, Al is the most detrimental to local order while boosting the shoulder associated with the connectivity-related twisting modes. In contrast, P causes the least disruption to local order, and has little effect on the connectivity-related shoulder. Na seems to cause disorder on short and intermediate length scales.

Fig. 4. $S(q)$ as a function of (*a*) impurity type and (*b*) density. In (*b*), the arrow tracks the increase in density.

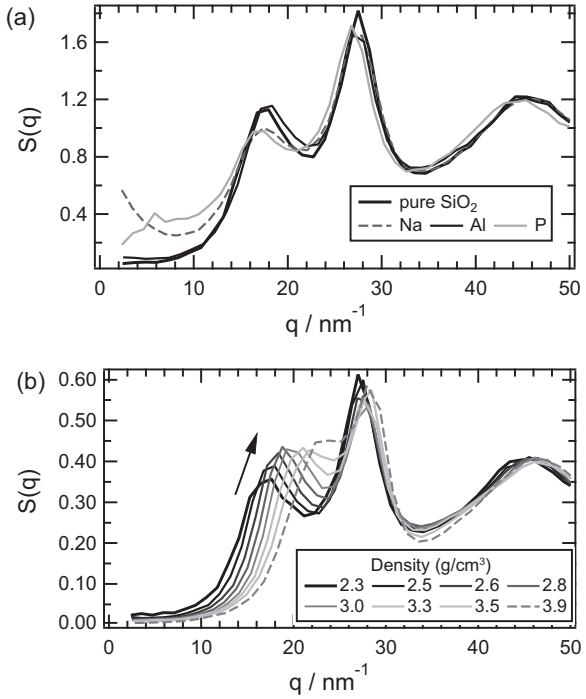

To provide more insight on the differences between the density-driven and substitutional impurities, we also track disorder through the radial distribution function, $g(r)$, and its integral, $n(r)$, which provide information about the coordination sphere. As shown in Fig. 3*a*, there is virtually no difference in $n(r)$ for Si–O when either Na or P is the substitutional impurity. Al substitutions produce slightly higher Si coordination numbers, as the more rapid rise in its $n(r)$ curve indicates. Figures 3*b*, 3*c* show how the different substitutional impurities are coordinated to the O and Si atoms, respectively. The P shows a very strong tendency to form PO_4 tetrahedra, whereas the oxygen environment around the Al is generally more variable in terms of both coordination number and in nearest neighbour distances. The Na–O coordination sphere is the most mixed, showing no evidence of plateaus in the $n(r)$ plot and the longest neighbour distances in $g(r)$. For the Si interactions with the substituted species, P–Si is remarkably similar to Si–Si order, which can be inferred from the similarity in $g(r)$ for Si–Si in pure SiO_2 compared with the $g(r)$ for Si–P. Al impurities tend to sit closer to Si atoms than do Na impurities, and the Si–impurity correlations become more quickly suppressed with increasing r for the Na compared with the Al or P systems.

Comparing Figs. 3*a* and 3*b* with Fig. 3*d* shows that the changes that occur in the Si–O environments with increasing Al content are the most like those we observe with increasing density. Figure 3*d* covers a wide range of densities, spanning a correspondingly larger change in the $g(r)$ peak distances and the coordination sphere, $n(r)$. However, for relatively moderate changes in density, the $n(r)$ trends look qualitatively similar to those for the Al–O $n(r)$ shown in Fig. 3*b*. These findings are consistent with the similarities in the VDOS data for Al substitutions (Fig. 2*a*) and density changes (Fig. 2*b*), including the changes in peak intensities between 1000 and 1200 cm^{-1} and the increase in the intensity of the shoulder region near 850 cm^{-1}.

The effects of substitutional impurities on long-range positional order are also evident in the Si–Si partial structure factor, $S(q)$ (Fig. 4*a*). The first sharp diffraction peak, occurring near

17 nm^{-1} in pure SiO_2 at 2.31 g/cm^3 and which we refer to as the network peak, arises in network-forming liquids as a result of structural correlations beyond nearest neighbours [2]. This peak merges with the nearest-neighbour peak at 27 nm^{-1} as density increases. It is surprising that the network peak is nearly identical for Al-substituted glass compared with pure SiO_2. These two different glasses also have similar low plateau values for low q, which indicates similar compressibility values and uniformity of Si ions [29]. These similarities suggest that Al does not introduce voids or other medium-length-scale disruptions to the silica structure, even though the $g(r)$ data indicate that it does disrupt local positional order. On the other hand, P and Na both show considerable change to the long-range positional order, with a depressed network peak. In addition, P has a slight shift to the $S(q)$ peak positions. Thus, even though P substitutes readily for Si because both prefer a tetrahedral O coordination environment, P still disrupts the medium-range network according to $S(q)$ trends.

The effects of increasing density on the long-range positional order (Fig. 4*b*) are that of preserving structural correlations between second-nearest neighbours but at increasingly smaller distances with increasing density, because the network peak is preserved but shifts to larger q values.

5. Conclusion

1. Local positional order is best preserved by P substitutions, but this occurs at the expense of long-range positional order.
2. Al substitutions disrupt local order, but enhance midrange order.
3. Density increases preserve structural correlations between second-nearest neighbours, but scales them to smaller distances.

VDOS helps us to pick out these trends rapidly and accurately, and thus should be utilized more in theoretical assessments of structural order across different length scales in glassy and amorphous materials.

Acknowledgements

Thanks to C. Harnum (funded through the Women In Science Engineering Summer Student Employment Program at Memorial University) for assistance with data processing. NSERC Discovery Grants and Canada Summer Jobs funds (KMP and ISV) provided stipend support for VRG, and ACEnet provided computational resources.

References

1. D. Ma, A.D. Stoica, and X.L. Wang. Nat. Mater. **8**, 30 (2009). doi:10.1038/nmat2340. PMID:19060888.
2. S.R. Elliott. Nature, **354**, 445 (1991). doi:10.1038/354445a0.
3. B. Chen, U. Werner-Zwanziger, M.L.F. Nascimento, L. Ghussn, E.D. Zanotto, and J.W. Zwanziger. J. Phys. Chem. C, **113**, 20725 (2009). doi:10.1021/jp907259e.
4. G. Ferlat, A.P. Seitsonen, M. Lazzeri, and F. Mauri. Nat. Mater. **11**, 925 (2012). doi:10.1038/nmat3416. PMID:22941329.
5. P.H. Poole, T. Grande, F. Sciortino, H.E. Stanley, and C.A. Angell. Comp. Mater. Sci. **4**, 373 (1995). doi:10.1016/0927-0256(95)00044-9.
6. I. Saika-Voivod and P.H. Poole. Adv. Chem. Phys. **152**, 373 (2013).
7. P.M. Dove, N. Han, A.F. Wallace, and J.J. De Yoreo. Proc. Natl. Acad. Sci. U.S.A. **105**, 9903 (2008). doi:10.1073/pnas.0803798105. PMID:18632576.
8. K.M. Poduska, L. Regev, E. Boaretto, L. Addadi, S. Weiner, L. Kronik, and S. Curtarolo. Adv. Mater. **23**, 550 (2011). PMID:21254262.
9. A. Pedone. J. Phys. Chem. C, **113**, 20773 (2009). doi:10.1021/jp9071263.
10. Y. Xiang, J. Du, M.M. Smedskjaer, and J.C. Mauro. J. Chem. Phys. **139**, 044507 (2013). doi:10.1063/1.4816378. PMID:23901993.
11. P. Gillet, P. McMillan, J. Schott, J. Badro, and A. Grzechnik. Geochim. Cosmochim. Acta, **60**, 3471 (1996). doi:10.1016/0016-7037(96)00178-0.
12. A.G. Kalampounias, S.N. Yannopoulos, and G.N. Papatheodorou. J. Chem. Phys. **124**, 014504 (2006). doi:10.1063/1.2136878.
13. A.G. Kalampounias, S.N. Yannopoulos, and G.N. Papatheodorou. J. Non-Cryst. Solids, **352**, 4619 (2006). doi:10.1016/j.jnoncrysol.2006.02.163.
14. S.N. Taraskin and S.R. Elliott. Phys. Rev. B, **56**, 8605 (1997). doi:10.1103/PhysRevB.56.8605.
15. H. Aguiar, J. Serra, P. González, and B. León. J. Non-Cryst. Solids, **355**, 475 (2009). doi:10.1016/j.jnoncrysol.2009.01.010.
16. H.J.C. Berendsen, D. van der Spoel, and R. van Druren Comput. Phys. Commun. **91**, 43 (1995). doi:10.1016/0010-4655(95)00042-E.
17. E. Lindahl, B. Hess, and D. van der Spoel J. Mol. Model. **7**, 306 (2001).
18. D. van der Spoel, E. Lindahl, B. Hess, G. Groenhof, A.E. Mark, and H.J.C. Berendsen. J. Comput. Chem. **26**, 1701 (2005). doi:10.1002/jcc.20291. PMID:16211538.
19. B. Hess, C. Kutzner, D. van der Spoel, and E. Lindahl. J. Chem. Theory Comput. **4**, 435 (2008). doi:10.1021/ct700301q.
20. B.W.H. van Beest, G.J. Kramer, and R.A. van Santen Phys. Rev. Lett. **64**, 1955 (1990). doi:10.1103/PhysRevLett.64.1955. PMID:10041537.
21. I. Saika-Voivod, F. Sciortino, and P.H. Poole. Phys. Rev. E, **69**, 041503 (2004). doi:10.1103/PhysRevE.69.041503.
22. J. Horbach and W. Kob. Phys. Rev. B, **60**, 3169 (1999). doi:10.1103/PhysRevB.60.3169.
23. I. Saika-Voivod, F. Sciortino, and P.H. Poole. Philos. Mag. **84**, 1437 (2004). doi:10.1080/14786430310001644198.
24. G.J. Kramer, A.J.M. de Man, and R.A. van Santen J. Am. Chem. Soc. **113**, 6435 (1991). doi:10.1021/ja00017a012.
25. M. Allen and D. Tildesley. Computer simulation of liquids. Oxford University Press, New York (1989).
26. S.N. Taraskin and S.R. Elliott. Physica B, 316–317, **81** (2002).
27. N.F. Richet. Physica B, **404**, 3799 (2009). doi:10.1016/j.physb.2009.06.146.
28. M. Bauchy. J. Chem. Phys. **137**, 044510 (2012). doi:10.1063/1.4738501. PMID:22852634.
29. M. Hejna, P.J. Steinhardt, and S. Torquato. Phys. Rev. B, **87**, 245204 (2013). doi:10.1103/PhysRevB.87.245204.